Arthritis & Rheumatology
Vol. 74, No. 2, February 2022, pp 212–222
DOI 10.1002/art.41950

American College of Rheumatology
Empowering Rheumatology Professionals

Activation of Hypothalamic AMP-Activated Protein Kinase Ameliorates Metabolic Complications of Experimental Arthritis

Patricia Seoane-Collazo,[1] Eva Rial-Pensado,[1] Ánxela Estévez-Salguero,[1] Edward Milbank,[1] Lucía García-Caballero,[2] Marcos Ríos,[1] Laura Liñares-Pose,[1] Morena Scotece,[3] Rosalía Gallego,[2] José Manuel Fernández-Real,[4] Rubén Nogueiras,[1] Carlos Diéguez,[1] Oreste Gualillo,[3] and Miguel López[1]

Objective. To investigate whether thermogenesis and the hypothalamus may be involved in the physiopathology of experimental arthritis (EA).

Methods. EA was induced in male Lewis rats by intradermal injection of Freund's complete adjuvant (CFA). Food intake, body weight, plasma cytokines, thermographic analysis, gene and protein expression of thermogenic markers in brown adipose tissue (BAT) and white adipose tissue (WAT), and hypothalamic AMP-activated protein kinase (AMPK) were analyzed. Virogenetic activation of hypothalamic AMPK was performed.

Results. We first demonstrated that EA was associated with increased BAT thermogenesis and browning of subcutaneous WAT leading to elevated energy expenditure. Moreover, rats experiencing EA showed inhibition of hypothalamic AMPK, a canonical energy sensor modulating energy homeostasis at the central level. Notably, specific genetic activation of AMPK in the ventromedial nucleus of the hypothalamus (a key site modulating energy metabolism) reversed the effect of EA on energy balance, brown fat, and browning, as well as promoting amelioration of synovial inflammation in experimental arthritis.

Conclusion. Overall, these data indicate that EA promotes a central catabolic state that can be targeted and reversed by the activation of hypothalamic AMPK. This might provide new therapeutic alternatives to treat rheumatoid arthritis (RA)–associated metabolic comorbidities, improving the overall prognosis in patients with RA.

INTRODUCTION

Rheumatoid arthritis (RA) is an autoimmune and chronic inflammatory disease that mainly affects the synovium but also induces systemic manifestations causing pain, swelling, stiffness, unsteadiness, and deformity. Of note, RA is frequently associated with fatigue, weakness, fever, and weight loss (1–3). The mechanisms underlying metabolic complications in RA are not well

The Centro Singular de Investigación en Medicina Molecular y Enfermedades Crónicas (CiMUS) is supported by the Xunta de Galicia (2016-2019, ED431G/05). The Centro de Investigación Biomédica en Red Fisiopatología de la Obesidad y Nutrición (CIBERobn) is an initiative of the Instituto de Salud Carlos III. Supported by the Xunta de Galicia (grants 2016-PG057 to Dr. Nogueiras, GPC IN607B2019/10 to Dr. Gualillo, and 2016-PG068 to Dr. López), the Ministerio de Economía y Competitividad (MINECO) co-funded by the FEDER Program of the European Union (grants BFU2017-90578-REDT/Adipoplast to Drs. Fernández-Real and López, RTI2018-099413-B-I00 to Dr. Nogueiras, BFU2017-87721-P to Dr. Diéguez, and RTI2018-101840-B-I00 to Dr. López), the Instituto de Salud Carlos III (grants PI15–01934 and PI18/0102224 to Dr. Fernández-Real and PI17/00409, PI20/00902, RD21/0002/0025, and RD16/0012/0014 to Dr. Gualillo), "la Caixa" Foundation (ID 100010434) (grant LCF/PR/HR19/52160022 to Dr. López), and the European Research Council (synergy grant-2019-WATCH- 810331 to Dr. Nogueiras). Dr. Seoane-Collazo's work was supported by the Xunta de Galicia (fellowship ED481B 2018/050) and the Horizon 2020 Research and Innovation Program of the European Union under the Marie Sklodowska-Curie actions. Drs. Nogueiras and López's work was supported in part by the Atresmedia Corporación. Dr. Nogueiras's work was supported in part by Fundación BBVA and the European Foundation for the Study of Diabetes. Dr. Gualillo's work was supported in part by the Horizon 2020 Research and Innovation Program of the European Union under the Marie Sklodowska-Curie actions (project no. 734899) and by the Xunta de Galicia through a research staff contract (ISCIII/SERGAS).

[1]Patricia Seoane-Collazo, PhD, Eva Rial-Pensado, PhD, Ánxela Estévez-Salguero, PhD, Edward Milbank, PhD, Marcos Ríos, PhD, Laura Liñares-Pose, PhD, Rubén Nogueiras, PhD, Carlos Diéguez, MD, PhD, Miguel López, PhD: Centro Singular de Investigación en Medicina Molecular y Enfermedades Crónicas, Universidade de Santiago de Compostela, Instituto de Investigación Sanitaria, and CIBERobn, Santiago de Compostela, Spain; [2]Lucía García-Caballero, DDS, PhD, Rosalía Gallego, MD, PhD: Universidade de Santiago de Compostela, Santiago de Compostela, Spain; [3]Morena Scotece, PhD, Oreste Gualillo, PharmD, PhD: SERGAS, Instituto de Investigación Sanitaria de Santiago, NEIRID Lab, and Santiago University Clinical Hospital, Santiago de Compostela, Spain; [4]José Manuel Fernández-Real, MD, PhD: CIBERobn, Santiago de Compostela, Spain, and Institut d'Investigació Biomèdica de Girona and Hospital Universitari de Girona Doctor Josep Trueta, Girona, Spain.

Drs. Seoane-Collazo, Rial-Pensado, and Estévez-Salguero contributed equally to this work.

Author disclosures are available at https://onlinelibrary.wiley.com/action/downloadSupplement?doi=10.1002%2Fart.41950&file=art41950-sup-0001-Disclosureform.pdf.

Address correspondence to Oreste Gualillo, PhD, SERGAS, Instituto de Investigación Sanitaria de Santiago, NEIRID Lab, Santiago University Clinical Hospital, Research Area, Laboratory no. 9, Building C, Level 2, Trav. Choupana sn, Santiago de Compostela 15706, Spain (email: oreste.gualillo@sergas.es), or to Miguel López, PhD, CiMUS, Santiago de Compostela, Galicia 15782, Spain (email: m.lopez@usc.es).

Submitted for publication October 26, 2020; accepted in revised form August 10, 2021.

understood, but a serious catabolic status, driven predominantly by proinflammatory cytokines, might be responsible for body cell mass loss, a common feature of RA (4,5). In fact, there is increasing evidence about the contribution of the dysregulation of adipose tissue to RA, in particular dysregulated secretion of adipokines (4–7).

Obesity can play a dual role in RA, both by exacerbating its development and as a result of the disease progression, in part due to the patient's inability to carry out physical exercise and thereby inducing weight gain, something that may also be boosted by certain drugs used in the management of the illness (1,8–10). There is a general consensus that obesity prevention is important in patients with RA since it improves pain perception and metabolic and cardiovascular risk, as well as favoring a better response to treatments, such as anti–tumor necrosis factor (TNF) (11) and anti–interleukin-6 (anti–IL-6) receptor antibody (12).

A link between RA and altered levels of energy balance modulators acting at the central level, such as ghrelin, leptin, and other adipokines, has also been described (1,6,7,13). Moreover, a substantial amount of data highlighted a close relationship between alterations in different neuronal populations, some of them hypothalamic, and experimental arthritis (EA) (14–18). However, whether a dysregulation of these hypothalamic mechanisms is a cause or a consequence of the disease or, more importantly, whether targeting these hypothalamic nuclei may have a positive impact on the development of EA, remains unclear. Here, we aimed to investigate whether the hypothalamus may be involved in the physiopathology of EA. We focused on AMP-activated protein kinase (AMPK) in a specific set of neurons located in the ventromedial nucleus of the hypothalamus (VMH), which recently emerged as a critical canonical mechanism controlling energy homeostasis (19,20). In this sense, current evidence has shown that inhibition of AMPK in steroidogenic factor 1 cells of the VMH leads to sympathetic nervous system–mediated activation of the brown adipose tissue (BAT) thermogenesis, leading to increased energy expenditure and feeding-independent weight loss (19–24). Notably, this mechanism mediates the actions of key thermogenic factors, such as thyroid hormones, bone morphogenetic protein 8B, estradiol, liraglutide receptor agonism, and nicotine (19–24).

Therefore, our aim was to investigate whether this central pathway might be involved in the metabolic alterations induced in an experimental model of arthritis. We used a model of EA induced by intradermal injection of Freund's complete adjuvant (CFA), which does not reflect every aspect of human RA but is a routinely used model and resembles some of the articular and extraarticular features of the disease (13,15,16).

MATERIALS AND METHODS

Animals and experimental protocols. Male Lewis rats (*Lew/OrlRj*, 200 gm, 6–7 weeks old; Janvier Labs) were used. Animals were housed under controlled light (12-hour light/dark cycle), temperature, and humidity conditions. The animals were allowed to freely drink water and were given a standard diet (SD) (Scientific Animal Food & Engineering: 3% fat, 60% carbohydrates, and 16% protein; Amersfoort) or a high-fat diet (HFD) (D12451: 45% fat, 35% carbohydrates, 20% protein; Research Diets, Inc.) for 3 weeks before the initiation of CFA-induced EA. All experiments and procedures were performed in agreement with International Law on Animal Experimentation and the USC Ethical Committee (project ID 15010/14/006 and 15012/2020/010).

CFA-induced EA. EA was induced by intradermal injection of CFA (0.1 ml suspension of *Mycobacterium tuberculosis* [13,15,16] [1 mg/ml] in sterile mineral oil; Sigma-Aldrich) into the dorsal side of the tail base; sham-treated animals were injected with the same volume of mineral oil. The evaluation of clinical arthritis was performed by the following methods: 1) histopathologic analysis of tibiotarsal sections on day 14, 2) measurement of the paw volume using a hydroplethysmometer (Ugo Basile), and 3) measurement of the edema volume change. Edema volume change was calculated using the difference of means in paw volume from SD-fed rats with CFA-induced EA versus SD-fed sham-treated rats or HFD-fed rats with CFA-induced EA versus HFD-fed sham-treated rats, respectively.

Stereotaxic microinjection of adenoviral expression vectors. Adenoviral vectors with green fluorescent protein (GFP) or constitutively active AMPKα1 (AMPKα1-CA) (ViraQuest) were delivered as previously described (21–23).

Indirect calorimetry. Animals were analyzed for energy expenditure, respiratory quotient, and locomotor activity using a calorimetric system (LabMaster; TSE Systems) as previously described (22–24). Rearing locomotor activity was analyzed by the number of bean break counts on the z-axis.

Temperature measurements. Skin temperature surrounding BAT and paw temperature were recorded with an infrared camera (B335: Compact Infrared Thermal Imaging Camera; FLIR) and analyzed with a specific software package (FLIR Tools Software), as previously described (22–24).

Blood biochemistry. Levels of TNF, IL-1, IL-6, IL-10, IL-17, and interferon-γ (IFNγ) were measured using Bio-Plex rat cytokine assays (Bio-Rad).

Real-time polymerase chain reaction (PCR). Real-time PCR (TaqMan; Applied Biosystems) was performed as previously described (21–23), using either of the following: 1) specific sets of primers/probes for peroxisome proliferator–activated receptor γ coactivator 1α (PGC-1α) (*Ppargc1a*; 5′-CGATCACCATATTC CAGGTCAAG-3′ [forward], 5′-CGATGTGTGCGGTGTCTGTAGT-3′ [reverse]; FAM-5′-AGGTCCCCAGGCAGTAGATCCTCT

TCAAGA-3′-TAMRA [probe]), or 2) commercially available and prevalidated TaqMan primer/probe sets for PGC-1β (*Ppargc1b*; assay no. Rn00598552_m1). Gene expression values were expressed in relation to the levels of hypoxanthine guanine phosphoribosyltransferase (5′-AGCCGACCGGTTCT GTCAT-3 ′ [forward], 5′-GGTCATAACCTGGTTCATCATCAC-3′ [reverse], FAM-5′-CGACCCTCAGTCCCAGCGTCGTGAT-3′-TAMRA [probe]).

Histology. Histologic samples were fixed in 10% neutral buffered formalin for 24 hours. For decalcification, the samples were immersed in a 10% formic solution in water (volume/volume; Sharlan) for 10 days at room temperature and subsequently embedded in paraffin routinely. Sections that were 4-μm thick were stained with hematoxylin and eosin (H&E) and imaged at 4× the original magnification using a slide scanner for digital pathology (PathScan Excilone).

Immunohistochemistry. Detection of uncoupling protein 1 (UCP-1) in white adipose tissue (WAT) was performed using an anti–UCP-1 antibody (1:500 dilution) (no. ab10983; Abcam) (22,24). Digital images were quantified using ImageJ version 1.44 (National Institutes of Health), as previously shown (22,24).

Western blotting. Protein lysates from the hypothalamus and BAT were subjected to sodium dodecyl sulfate–polyacrylamide gel electrophoresis, electrotransferred, and probed with antibodies against UCP-1 (1:10,000 dilution) (no. ab10983; Abcam), β-actin (1:5,000 dilution) (no. A5316; Sigma), α-tubulin (1:5,000 dilution) (no. T5168; Sigma), AMPKα1 (1:1,000 dilution) (no. 07-350; Merck Millipore), AMPKα2 (1:1,000 dilution) (no. 07-363; Merck Millipore), phosphorylated AMPKα (pAMPKα; threonine^{172}) (1:1,000 dilution) (no. 2535S; Cell Signaling), phosphorylated acetyl-coenzyme A carboxylase α (p-ACCα; Serine^{79}) (1:1,000 dilution) (no. 3661; Cell Signaling), ACCα (1:1,000 dilution) (no. 04-322; Merck Millipore), and fatty acid synthase (FAS; 1:1,000 dilution) (no. 610962; BD). Band signals were quantified by densitometry using ImageJ version 1.44 (21–23). Values were expressed in relation to β-actin (hypothalamus) or α-tubulin (BAT). In all figures showing images of gels, the bands for each picture were obtained from the same gel, although they may have been spliced for clarity.

Statistical analysis. Data are expressed as the mean ± SEM. Statistical significance was determined by Student's *t*-test (2 groups) or analysis of variance (≥2 groups) followed by a post hoc Tukey test. *P* values less than 0.05 were considered significant. The correlation between parameters was evaluated with Pearson's correlation coefficient.

Data availability. All data generated and analyzed in this study are available upon reasonable request. Access to data generated in this study is available upon request from the corresponding authors.

RESULTS

Occurrence of CFA-induced EA independent of body weight. First, Lewis rats were fed an a SD or HFD for 3 weeks. Animals with diet-induced obesity showed a significant increase in body weight (mean ± SEM 277.30 ± 4.023 gm for SD-fed rats versus 301.30 ± 3.2 gm for HFD-fed rats;

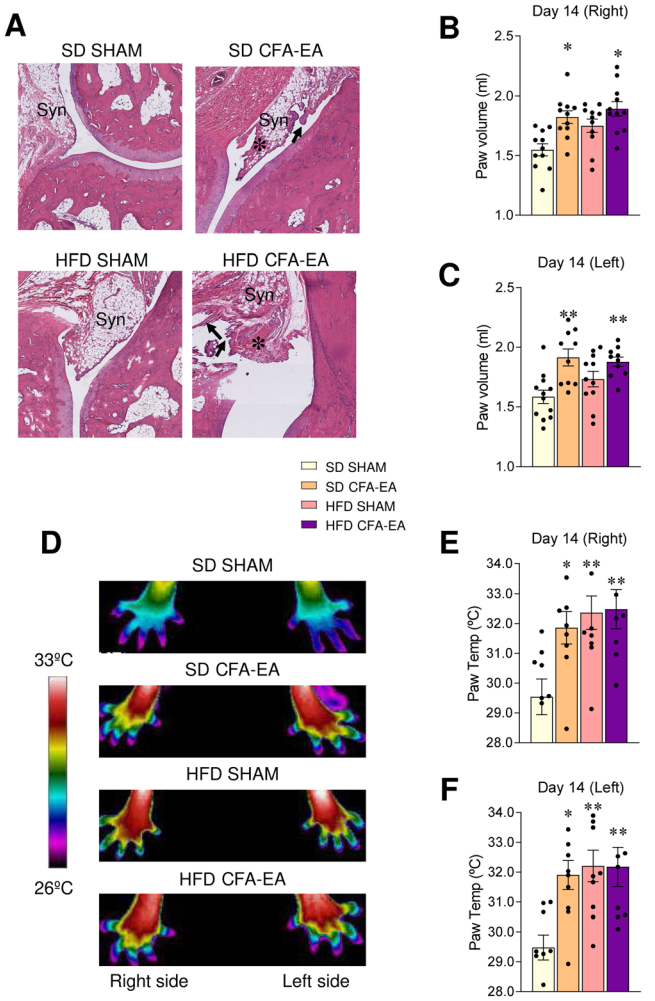

Figure 1. Experimental arthritis (EA) induction with Freund's complete adjuvant (CFA) in rats fed a standard diet (SD) or high-fat diet (HFD). **A,** Representative sections of the tibiotarsal joints of SD-fed or HFD-fed rats intradermally treated with mineral oil or CFA. In the joints of rats with CFA-induced EA, synovia (Syn) show hyperplasia, with papillary projections (**arrows**) and fibrosis (**asterisks**) (hematoxylin and eosin staining at 4× original magnification). **B–F**, Paw volume in right (**B**) and left (**C**) posterior paws, and representative thermal images (**D**) and paw temperature in right (**E**) and left (**F**) posterior paws of SD-fed or HFD-fed rats intradermally treated with mineral oil or CFA. Symbols represent individual rats (n = 7–12 rats per group). Bars show the mean ± SEM. * = $P < 0.05$; ** = $P < 0.01$ versus SD-fed sham-treated animals, by analysis of variance.

$P < 0.001$). Next, CFA was inoculated into the dorsal side of the tail base. Our data show that both SD-fed rats with CFA-induced EA and HFD-fed rats with CFA-induced EA developed signs of inflammation, as demonstrated by histologic analysis showing normal cartilage and bone structures in the H&E–stained tibiotarsal sections of sham-treated animals fed an SD or HFD (Figure 1A). In addition, we observed synovial hyperplasia, narrowing of joint space, and cartilage and bone destruction in the arthritic tibiotarsal joints of SD-fed rats with CFA-induced EA and HFD-fed rats with CFA-induced EA (Figure 1A). Consistent with this, the rats displayed an increase in the right and left posterior paw volume 7 days after the adjuvant injection, reaching maximum levels on day 14 (peak phase) and improving on day 28 (recovery phase) (Figures 1B and C and Supplementary Figures 1A–D, available on the *Arthritis & Rheumatology* website at http://onlinelibrary.wiley.com/doi/10.1002/art.41950/abstract). The analysis of edema volume confirmed those data, showing that maximal volume changes mainly occurred on days 7–14 (Supplementary Figures 1E and F) in SD-fed and HFD-fed rats.

Rats with CFA-induced EA also showed an incapacity to bend the ankle and developed nodules at the base of the tail and ears (data not shown). To add more insight to the inflammatory status of the animals, we analyzed the temperature of the paws using infrared thermography. Our data showed that both an HFD feeding regimen and inoculation with CFA induced an increase of both right and left paw temperature (Figures 1D–F), which is suggestive of inflammation.

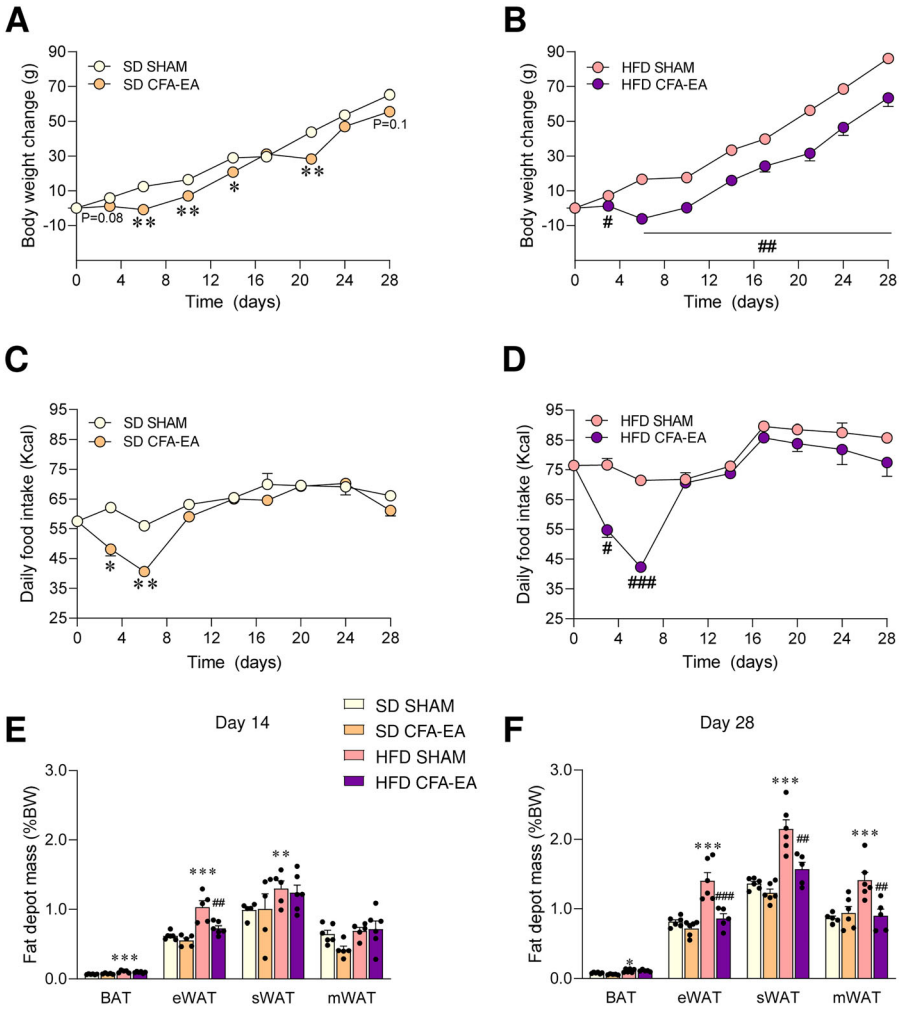

Figure 2. Effect of CFA-induced EA on energy balance in SD-fed or HFD-fed rats. Body weight change (**A** and **B**), daily food intake (**C** and **D**), and fat depot masses at 14 days (**E**) and 28 days (**F**) after intradermal treatment with mineral oil or CFA in SD-fed or HFD-fed rats. Symbols represent individual rats (n = 5–12 rats per group at 14 days and 5–6 rats per group at 28 days). Bars show the mean ± SEM. In **A–D**, *P* values were determined using Student's *t*-test, and in **E** and **F**, analysis of variance was used. * = $P < 0.05$; ** = $P < 0.01$; *** = $P < 0.001$ versus SD-fed sham-treated animals. # = $P < 0.05$; ## = $P < 0.01$; ### = $P < 0.001$ versus HFD-fed sham-treated animals. %BW = percentage body weight; BAT = brown adipose tissue; eWAT = epididymal white adipose tissue; mWAT = mesenteric WAT; sWAT = subcutaneous WAT (see Figure 1 for other definitions). Color figure can be viewed in the online issue, which is available at http://onlinelibrary.wiley.com/doi/10.1002/art.41950/abstract.

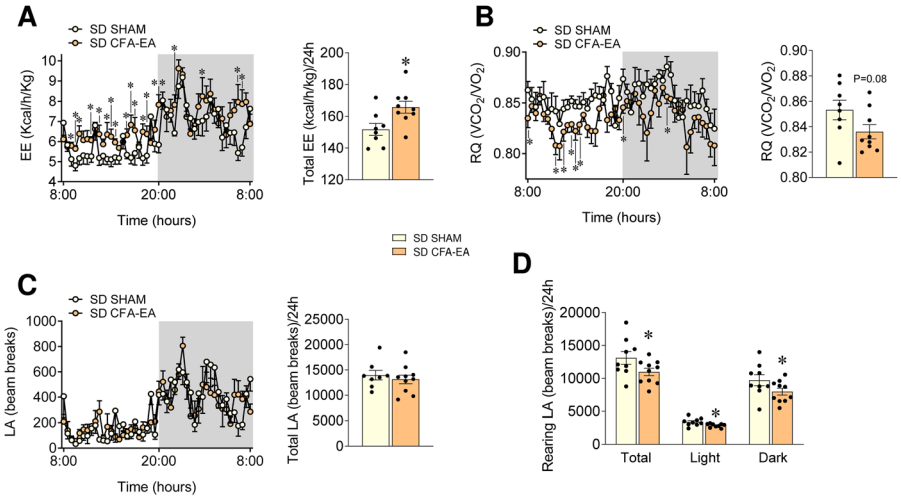

Figure 3. Effect of CFA-induced EA on energy expenditure (EE), respiratory quotient (RQ), and locomotor activity (LA) in SD-fed rats. EE and total EE (**A**), RQ and average RQ (**B**), LA and total LA (**C**), and rearing LA (**D**) in SD-fed rats intradermally treated with mineral oil or CFA. Symbols represent individual rats (n = 8–10 rats per group). Bars show the mean ± SEM. * = $P < 0.05$; ** = $P < 0.01$ versus sham-treated animals, by Student's *t*-test. See Figure 1 for other definitions. Color figure can be viewed in the online issue, which is available at http://onlinelibrary.wiley.com/doi/10.1002/art.41950/abstract.

Negative energy balance state resulting from CFA-induced EA. Analysis of body weight changes demonstrated that both SD-fed and HFD-fed rats with CFA-induced EA showed a negative energy balance, as revealed by weight loss, which was more evident in the HFD group (Figures 2A and B), as well as hypophagia during the first week (Figures 2C and D). This was associated with decreased adiposity, and we observed reduced epididymal WAT (on days 14 and 28), subcutaneous WAT (from the inguinal area, on day 28), and mesenteric WAT (on day 28) pad masses in HFD-fed rats but not in SD-fed rats (Figures 2E and F). Notably, during the peak phase (day 14), no correlation was found between initial body weight and body weight loss in the animals with CFA-induced EA (Supplementary Figure 2A, http://onlinelibrary.wiley.com/doi/10.1002/art.41950/abstract), although there was a nonsignificant trend in the recovery phase (day 28) (Supplementary Figure 2B). Overall, these data indicate that a higher body weight prior to CFA-induced EA does not have any beneficial effect either during the peak of the illness or in the recovery phase and that CFA-induced EA is very similar in both diet-induced obese (HFD) and lean (SD) rodents. On the contrary, according to the obtained data, HFD might worsen the energy balance outcome in the EA model.

Increased energy expenditure in CFA-induced EA. Considering the changes observed in body weight, which could not be simply explained by changes in food intake, we decided to assess energy expenditure–related mechanisms. Therefore, we performed an indirect calorimetry analysis of sham-treated and CFA-induced EA groups fed with SD or HFD. Our data showed that SD-fed rats and HFD-fed rats with CFA-induced EA had a higher energy expenditure and lower respiratory quotient (indicative of higher lipid mobilization) than their respective sham-treated controls (Figures 3A and B and Supplementary Figures 3A and B, http://onlinelibrary.wiley.com/doi/10.1002/art.41950/abstract), while no changes in total locomotor activity were detected (Figures 3C and Supplementary Figure 3C). Of note, rearing locomotor activity was decreased in experimental animals, indicative of difficulties in standing over the hind legs (Figure 3D and Supplementary Figure 3D).

BAT thermogenesis and WAT browning in CFA-induced EA. Next, we analyzed the BAT in rats with CFA-induced EA. Our data showed a significant increase in the protein levels of UCP-1 (a mitochondrial carrier protein located in BAT that generates heat by non-shivering thermogenesis) in the BAT of rats with CFA-induced EA, on days 14 and 28 independently of diet (Figure 4A and Supplementary Figures 4A–C, http://onlinelibrary.wiley.com/doi/10.1002/art.41950/abstract). Further BAT analysis showed that the levels of messenger RNA for *Ppargc1a* (the gene for PGC-1α and a key transcription factor regulating *Ucp1* gene expression), but not *Ppargc1b*, were also increased on day 14 in SD-fed rats with CFA-induced EA (Figure 4B). In accordance with these data, thermographic analysis proved that SD-fed rats with CFA-induced EA displayed an increased BAT temperature, which was indicative of augmented brown fat thermogenesis (Figure 4C). Activation of beige/brite ("brown-in-white") adipocytes in the WAT, a process known as browning, is responsible for a significant increase in total energy expenditure (25,26). However, to date, no data have linked RA to the browning of WAT. Our histologic analysis of subcutaneous WAT showed that SD-fed rats with CFA-induced EA exhibited increased UCP-1 immunostaining (Figures 4D and E) and

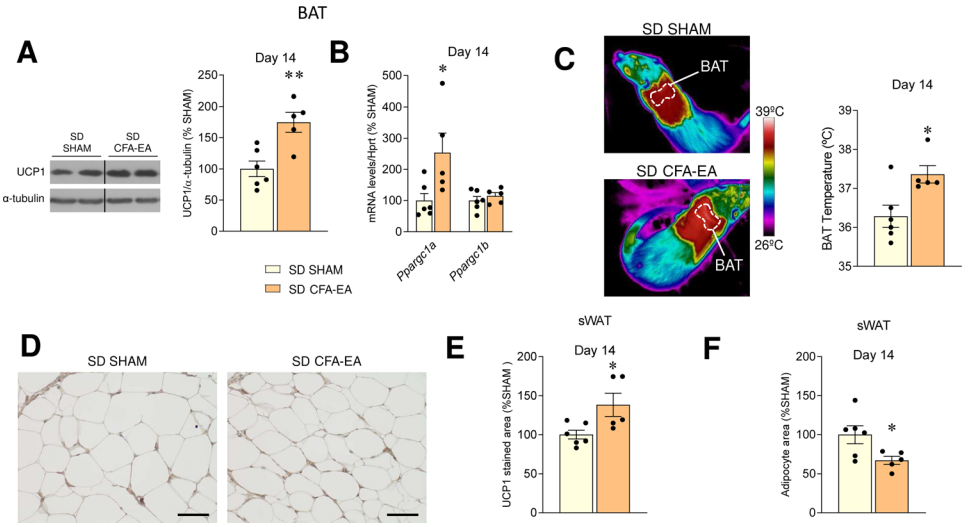

Figure 4. Effect of CFA-induced EA on brown adipose tissue (BAT) and subcutaneous white adipose tissue (sWAT). Representative Western blot images and levels of BAT uncoupling protein 1 (UCP-1) (**A**), BAT levels of mRNA for *Ppargc1a* and *Ppargc1b* (**B**), representative thermal images and levels of BAT temperature (**C**), representative immunohistochemical staining with an anti–UCP-1 antibody (bars = 100 μm) (**D**), UCP-1–stained area (**E**), and adipocyte area (**F**) on day 14 posttreatment in SD-fed rats intradermally treated with mineral oil or CFA. For the Western blot analysis, representative images for all proteins are shown; all bands for each picture were obtained from the same gel, but they may be spliced for clarity, which is indicated by vertical lines. Symbols represent individual rats (n = 5–6 rats per group). Bars show the mean ± SEM. * = $P < 0.05$; ** = $P < 0.01$ versus SD-fed sham-treated animals, by Student's *t*-test. See Figure 1 for other definitions. Color figure can be viewed in the online issue, which is available at http://onlinelibrary.wiley.com/doi/10.1002/art.41950/abstract.

decreased adipocyte area (Figures 4D and F), which are indicative of browning.

Central effects of CFA-induced EA on energy balance dependent on AMPK in the VMH. Rats with CFA-induced EA showed decreased AMPK activity, as demonstrated by reduced levels of pAMPKα and its downstream target p-ACCα in the hypothalamus (Figure 5A and Supplementary Figures 5A–C, http://onlinelibrary.wiley.com/doi/10.1002/art.41950/abstract). Consistent with those findings, protein levels of FAS, which is negatively regulated by AMPK (27), were elevated in the hypothalamus of animals with CFA-induced EA (Figure 5A and Supplementary Figures 5A–C). Notably, as it has been described in other models of hypothalamic AMPK inhibition (21–23), decreased pAMPK was associated with reduced levels (or a trend toward reduction) of the AMPKα1, but not AMPKα2, subunit (Figure 5A and Supplementary Figures 5A–C).

We hypothesized that the negative energy balance that characterized EA-induced weight loss might be mediated by the specific inhibition of AMPK in the VMH, a key mechanism regulating thermogenesis (19–24). To evaluate this, adenoviruses encoding either for an AMPKα1-CA or a GFP control vector were injected stereotaxically into the VMH in rats with CFA-induced EA. First, we induced EA using CFA as indicated above and checked the progression of the illness on day 8 (body weight change mean ± SEM 12.57 ± 3.36 gm for sham-treated controls versus −2.21 ± 2.27 gm for rats with CFA-induced EA; $P < 0.001$). On day 9, we injected the adenovirus to pair the effect of the adenovirus with the peak of EA. The AMPKα1-CA adenovirus was previously validated (21–23) and induced a significant increase in p-ACCα protein levels within the VMH (mean ± SEM 100 ± 18.3 for GFP-injected rats with CFA-induced EA versus 170.7 ± 25.7 for AMPKα1-CA–injected rats with CFA-induced EA; $P < 0.05$). Overexpression of AMPKα1-CA in the VMH, confirmed by GFP immunofluorescence (21–23) (data not shown), promoted an overall improvement in the inflammatory state of the rats, as demonstrated by reduced tissue swelling and ankylosis in the paws and tail as well as fur aspect in comparison with the GFP-injected control rats (Figure 5B). AMPKα1-CA also blunted the weight loss caused by CFA injection and displayed an increased food intake (Figures 5C and D). Notably, this effect was associated with reversal of the CFA-induced thermogenesis (Figures 6A) and browning of subcutaneous WAT, as demonstrated by decreased UCP-1 staining (Figures 6B and C) and enhanced adipocyte area (Figures 6B and D) in CFA-treated rats receiving AMPKα1-CA adenoviruses in the VMH for 6 days, compared to CFA-treated rats treated with control GFP adenoviruses. AMPKα1-CA adenoviruses did not impact any of the aforementioned parameters when administrated in sham-treated rats (data not shown).

Reversal of CFA-induced EA–associated inflammatory phenotype via activation of AMPK in the VMH. Finally, we investigated whether, besides energy balance, the AMPKα1-CA adenovirus injected into the VMH could reverse the overall inflammatory state that characterizes CFA-induced

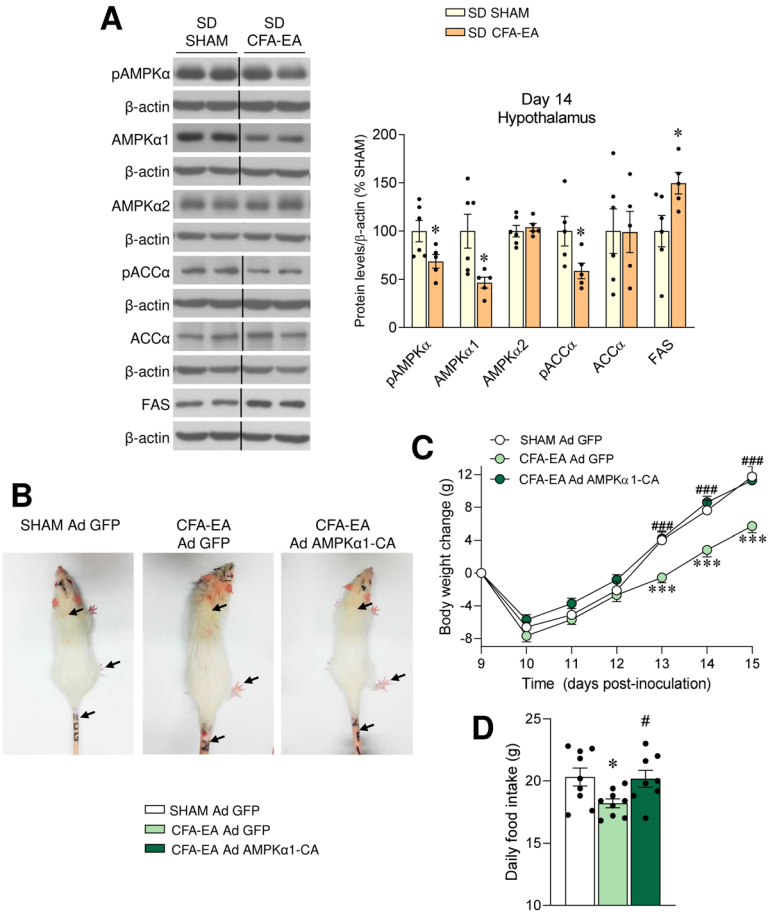

Figure 5. Effect of adenoviral constitutively active AMP-activated protein kinase α1 (AMPKα1-CA) overexpression in the ventromedial nucleus of the hypothalamus (VMH) on energy balance in rats with CFA-induced EA. **A**, Representative Western blot images and hypothalamic protein levels of the AMPK pathway on day 14 posttreatment in SD-fed rats intradermally treated with mineral oil or CFA. **B–D**, Photographs of a representative rat in each group (**B**), body weight change (**C**), and daily food intake (**D**) in SD-fed rats intradermally treated with mineral oil or CFA and stereotaxically injected with green fluorescent protein (GFP) or AMPKα1-CA adenovirus (Ad) in the VMH. Experiments including the sham-treated animals injected with AMPKα1 were performed, but they have been excluded in the graphs for simplification. In **B, arrows** show tissue swelling in the paws and tail as well as fur aspect. For the Western blot analysis, representative images for all proteins are shown; all bands for each picture were obtained from the same gel, but they may be spliced for clarity, which is indicated by vertical lines. Symbols represent individual rats (n = 5–6 rats per group in **A** and 8–10 rats per group in **B–D**). Bars show the mean ± SEM. In **A**, *P* values were determined using Student's *t*-test, and in **C** and **D**, analysis of variance was used. * = $P < 0.05$; *** = $P < 0.001$ versus sham-treated animals with or without GFP injection. # = $P < 0.05$; ### = $P < 0.001$ versus rats with CFA-induced EA injected with GFP. p-ACCα = phosphorylated acetyl-coenzyme A carboxylase α; FAS = fatty acid synthase (see Figure 1 for other definitions). Color figure can be viewed in the online issue, which is available at http://onlinelibrary.wiley.com/doi/10.1002/art.41950/abstract.

EA. Our data showed that, in rats with CFA-induced EA, the circulating levels of inflammatory cytokines, namely TNF, IL-1β, IL-6, IFNγ, and IL-17, were higher, while levels of antiinflammatory cytokine IL-10 were lower (Figure 6E). Notably, when treatment with AMPKα1-CA was administered into the VMH, the inflammatory status observed in rats with CFA-induced EA was improved. AMPKα1-CA adenoviruses did not impact the aforementioned parameters when administrated to sham-treated rats (data not shown). Correlation analyses of those effects also demonstrated that circulating levels of TNF, IL-1, and IL-6 were negatively associated with changes in body weight and/or food intake (Supplementary Table 1, http://onlinelibrary.wiley.com/doi/10.1002/art.41950/abstract).

DISCUSSION

The relationship between obesity and several inflammatory and autoimmune diseases, such as RA, has been broadly studied over the last decades. However, the underlying mechanism is still under debate. There is a general consensus that both diseases are associated with an imbalance between proinflammatory and antiinflammatory cytokines contributing to the onset and progression of RA and obesity (4,5). Therefore, in this study we aimed to clarify whether obesity could influence RA and to uncover the molecular mechanism responsible for RA-induced altered energy balance. With this in mind, we induced EA by CFA inoculation (13,15,16) in a rat model (those fed a control diet [SD] versus

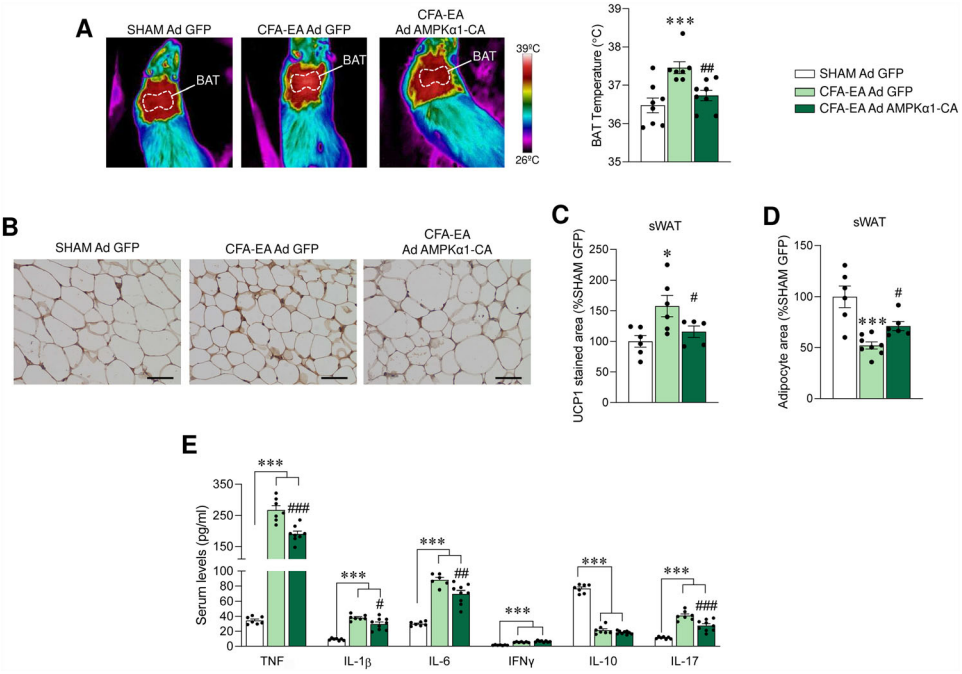

Figure 6. Effect of adenoviral constitutively active AMP-activated protein kinase α1 (AMPKα1-CA) overexpression in the ventromedial nucleus of the hypothalamus (VMH) in rats with CFA-induced EA on energy balance and inflammatory state. Shown are representative thermal images and brown adipose tissue (BAT) temperature (**A**), representative immunohistochemical images of subcutaneous white adipose tissue stained with anti–uncoupling protein 1 (anti–UCP-1) antibody (bars = 100 μm) (**B**), UCP-1–stained area (**C**), adipocyte area (**D**), and circulating levels of tumor necrosis factor (TNF), interleukin-1 (IL-1), IL-6, interferon-γ (IFNγ), IL-10, and IL-17 (**E**) in SD-fed rats intradermally treated with mineral oil or CFA and stereotaxically injected with green fluorescent protein (GFP) or AMPKα1-CA adenovirus (Ad) in the VMH. Experiments including the sham-treated animals injected with AMPKα1 were performed, but they have been excluded in the graphs for simplification. Symbols represent individual rats (n = 6–9 rats per group). Bars show the mean ± SEM. * = $P < 0.05$; *** = $P < 0.001$ versus sham-treated animals with GFP injection, by analysis of variance (ANOVA). # = $P < 0.05$; ## = $P < 0.01$; ### = $P < 0.001$ versus rats with CFA-induced EA injected with GFP, by ANOVA. See Figure 1 for other definitions.

those fed an HFD) and also assessed its impact on peripheral and central mechanisms regulating energy balance. We focused specifically on BAT thermogenesis, since it is known that induction of EA by CFA is characterized, in some cases, by increased energy expenditure (28,29). Furthermore, it is known that RA is characterized by weight loss and wasting, a state known as rheumatoid cachexia (RC), but the mechanism by which some RA patients lose weight is not well defined and may be multifactorial (1–3). A similar situation is present in cancer-induced cachexia, where activation of brown fat thermogenesis has been described (30–33).

The phenotype observed in our preclinical model is consistent with the definition of pre-cachexia, since it fulfils the features required to be present in patients with an underlying disease: chronic and systemic inflammation, hypophagia, and weight loss (34). However, it should be acknowledged that there are some clear differences between cachexia induced by other diseases, such as cancer, and RC. In classic cachexia, loss of body weight, due to muscle and fat loss, is a common feature. These outcomes are consistent with data showing increased resting energy expenditure induced by BAT activation (30–33) or WAT browning (35–37), in both rodent models of cachexia and in patients with cachexia. In contrast, in RC, for which a consensus diagnostic criterion does not exist, the loss of body weight and adiposity rarely occurs (38,39).

Our data showed that both lean and obese rats displayed a similar increase in paw volume after EA induction. No correlation was found between body weight and body weight loss. Remarkably, although both SD-fed and HFD-fed animals with CFA-induced EA displayed initial hypophagia, they restored their food intake after the peak of the illness; however, while SD-fed rats with CFA-induced EA were able to show a progressive body weight recovery, HFD-fed rats with CFA-induced EA failed to recuperate their body weight and continued to lose body weight and fat masses. To further improve our understanding of EA-induced alterations in energy balance, we assessed the effect of CFA-induced EA on BAT thermogenesis. We found a marked activation of BAT in all the stages of EA, in both SD-fed and HFD-fed animals, as shown by increased BAT temperature and/or increased levels of UCP-1 in brown fat, as well as browning of WAT.

Several mechanisms could explain this increased thermogenic tone in our experimental EA model, acting centrally or

directly on brown and white adipocytes. For example, it is known that cancer cachexia–induced browning is dependent on IL-6 (35). However, considering that the proinflammatory milieu represses the thermogenic activity of brown and beige fat via cytokines that inhibit noradrenergic signaling (25), central effects might be more important than direct peripheral actions on adipose cells. Given that AMPK in different hypothalamic neuronal populations regulates whole-body energy homeostasis, from feeding to BAT thermogenesis and browning of WAT (19,20,23,40), we next investigated the effect of EA in this pathway. Our data revealed that VMH AMPK is decreased in EA. Next, we investigated whether this effect was mechanistically associated with EA-induced actions on energy balance. Thus, we targeted AMPKα1 in the VMH, a nucleus where this catalytic subunit has been involved in both the modulation of feeding and BAT thermogenesis (19,20,27).

Our data showed that specific VMH AMPK activation using virogenetic strategies was enough to ameliorate the negative energy balance included by CFA-induced EA. Remarkably, besides body weight gain, restored feeding, and diminished BAT and browning tones, AMPKα1 activation in the VMH decreased the circulating levels of inflammatory cytokines, as well as improving the physical appearance of the animals. These later effects are quite relevant since it is assumed that proinflammatory cytokines are at the root of some of the most serious consequences of RA (4,5). In this sense, the mechanisms underlying metabolic complications in RA are unclear, although proinflammatory cytokines might also be responsible for the loss of body cell mass (4,5). In addition, the link between the hypothalamic AMPK axis and the inflammatory status raises very interesting pathophysiologic as well as physiologic questions. It is known that inflammation of tissues is under neural control, involving the neuroendocrine, sympathetic, and central nervous systems (18,41). Data from the 1990s had already demonstrated an association between sympathetic ganglia and the pathogenesis of EA (42,43). Of note, CFA-induced EA in Lewis rats has been linked to changes in the sympathetic nerves in the spleen and is also responsible for the activation of immune cells in the red pulp of that organ (44,45).

Remarkably, the spinal BAT sympathetic preganglionic neurons in the intermediolateral nucleus of the thoracolumbar spinal cord are in the same area as those innervating the spleen (46,47). Thus, activation of the same centers may promote both BAT thermogenesis and immune activation in the spleen. This connection is functionally supported by our data and a recent report showing that propranolol (a nonselective beta blocker) promotes, in addition to antiarrhythmic effects, a systemic antiinflammatory action in a model of collagen-induced arthritis in Lewis rats (48). Overall, this evidence seems to indicate that reduced sympathetic tone ameliorates EA symptoms, offering a possible alternative mechanism to the antiinflammatory effect of AMPKα1 adenoviral treatment in the VMH.

To our knowledge, this is the first study linking the canonical hypothalamic AMPK–BAT/WAT axis to the development of the symptoms of a systemic disease, such as RA. This is relevant because targeting hypothalamic AMPK, which has been proposed as a potential therapy for obesity (19), may also be a possible strategy to ameliorate the negative energy balance and to improve the inflammatory state associated with RA. In this sense, recent and profuse evidence has shown that metformin, a drug administered for the treatment of type 2 diabetes mellitus that activates AMPK, promotes metabolic improvement in RA patients and in animal models of pharmacologically induced and autoimmune arthritis (49,50).

In summary, our data show that negative energy balance caused by CFA-induced EA is independent of initial body weight, and it is associated with VMH AMPK–mediated activation of BAT thermogenesis and browning. Notably, activation of AMPK in the VMH not only ameliorates the metabolic outcome in CFA-induced EA but also improves the inflammatory status of the animals. Taken together, these findings provide new mechanistic insight into the pathophysiology of RA and suggest new therapeutic strategies for its possible clinical management and treatment.

AUTHOR CONTRIBUTIONS

All authors were involved in drafting the article or revising it critically for important intellectual content, and all authors approved the final version to be published. Dr. López, who is the lead author, had full access to all of the data in the study and takes responsibility for the integrity of the data and the accuracy of the data analysis.

Study conception and design. Seoane-Collazo, Rial-Pensado, Estévez-Salguero, Nogueiras, Diéguez, Gualillo, López.

Acquisition of data. Seoane-Collazo, Rial-Pensado, Estévez-Salguero, Milbank, García-Caballero, Ríos, Liñares-Pose, Scotece, Gallego, Gualillo, López.

Analysis and interpretation of data. Seoane-Collazo, Rial-Pensado, Estévez-Salguero, Milbank, Ríos, Fernández-Real, Nogueiras, Diéguez, Gualillo, López.

REFERENCES

1. Kerekes G, Nurmohamed MT, Gonzalez-Gay MA, Seres I, Paragh G, Kardos Z, et al. Rheumatoid arthritis and metabolic syndrome [review]. Nat Rev Rheumatol 2014;10:691–6.
2. Abella V, Scotece M, Conde J, Pino J, Gonzalez-Gay MA, Gomez-Reino JJ, et al. Leptin in the interplay of inflammation, metabolism and immune system disorders [review]. Nat Rev Rheumatol 2017;13:100–9.
3. Chen Z, Bozec A, Ramming A, Schett G. Anti-inflammatory and immune-regulatory cytokines in rheumatoid arthritis [review]. Nat Rev Rheumatol 2019;15:9–17.
4. Arshad A, Rashid R, Benjamin K. The effect of disease activity on fat-free mass and resting energy expenditure in patients with rheumatoid arthritis versus noninflammatory arthropathies/soft tissue rheumatism. Mod Rheumatol 2007;17:470–5.
5. Conde J, Scotece M, Lopez V, Gomez R, Lago F, Pino J, et al. Adipokines: novel players in rheumatic diseases [review]. Discov Med 2013; 15:73–83.
6. Procaccini C, Pucino V, Mantzoros CS, Matarese G. Leptin in autoimmune diseases [review]. Metabolism 2015;64:92–104.

7. La Cava A. Leptin in inflammation and autoimmunity [review]. Cytokine 2017;98:51–8.
8. Sattar N, McInnes IB. Rheumatoid arthritis: debunking the obesity-mortality paradox in RA. Nat Rev Rheumatol 2015;11:445–6.
9. George MD, Baker JF. The obesity epidemic and consequences for rheumatoid arthritis care [review]. Curr Rheumatol Rep 2016;18:6.
10. Procaccini C, Carbone F, Galgani M, La Rocca C, De Rosa V, Cassano S, et al. Obesity and susceptibility to autoimmune diseases [review]. Expert Rev Clin Immunol 2011;7:287–94.
11. Thomson TM, Lescarbeau RM, Drubin DA, Laifenfeld D, de Graaf D, Fryburg DA, et al. Blood-based identification of non-responders to anti-TNF therapy in rheumatoid arthritis. BMC Med Genomics 2015; 8:26.
12. Tournadre A, Pereira B, Dutheil F, Giraud C, Courteix D, Sapin V, et al. Changes in body composition and metabolic profile during interleukin 6 inhibition in rheumatoid arthritis. J Cachexia Sarcopenia Muscle 2017;8:639–46.
13. Otero M, Nogueiras R, Lago F, Dieguez C, Gomez-Reino JJ, Gualillo O. Chronic inflammation modulates ghrelin levels in humans and rats. Rheumatology (Oxford) 2004;43:306–10.
14. Cutolo M, Foppiani L, Minuto F. Hypothalamic-pituitary-adrenal axis impairment in the pathogenesis of rheumatoid arthritis and polymyalgia rheumatica. J Endocrinol Invest 2002;25 l:19–23.
15. Stofkova A, Haluzik M, Zelezna B, Kiss A, Skurlova M, Lacinova Z, et al. Enhanced expressions of mRNA for neuropeptide Y and interleukin 1 β in hypothalamic arcuate nuclei during adjuvant arthritis-induced anorexia in Lewis rats. Neuroimmunomodulation 2009;16: 377–84.
16. Skurlova M, Stofkova A, Kiss A, Belacek J, Pecha O, Deykun K, et al. Transient anorexia, hyper-nociception and cognitive impairment in early adjuvant arthritis in rats. Endocr Regul 2010;44:165–73.
17. Chikanza IC, Petrou P, Chrousos G. Perturbations of arginine vasopressin secretion during inflammatory stress: pathophysiologic implications [review]. Ann N Y Acad Sci 2000;917:825–34.
18. Bassi GS, Dias DP, Franchin M, Talbot J, Reis DG, Menezes GB, et al. Modulation of experimental arthritis by vagal sensory and central brain stimulation. Brain Behav Immun 2017;64:330–43.
19. López M, Nogueiras R, Tena-Sempere M, Diéguez C. Hypothalamic AMPK: a canonical regulator of whole-body energy balance [review]. Nat Rev Endocrinol 2016;12:421–32.
20. López M. AMPK wars: the VMH strikes back, return of the PVH. Trends Endocrinol Metab 2018;29:135–7.
21. López M, Varela L, Vázquez MJ, Rodríguez-Cuenca S, González CR, Velagapudi VR, et al. Hypothalamic AMPK and fatty acid metabolism mediate thyroid regulation of energy balance. Nat Med 2010;16: 1001–8.
22. Martins L, Seoane-Collazo P, Contreras C, González-García I, Martínez-Sánchez N, González F, et al. A functional link between AMPK and orexin mediates the effect of BMP8B on energy balance. Cell Rep 2016;16:2231–42.
23. Martínez-Sánchez N, Seoane-Collazo P, Contreras C, Varela L, Villarroya J, Rial-Pensado E, et al. Hypothalamic AMPK-ER stress-JNK1 axis mediates the central actions of thyroid hormones on energy balance. Cell Metab 2017;26:212–29.
24. Seoane-Collazo P, Roa J, Rial-Pensado E, Liñares-Pose L, Beiroa D, Ruíz-Pino F, et al. SF1-Specific AMPKα1 deletion protects against diet-induced obesity. Diabetes 2018;67:2213–26.
25. Villarroya F, Cereijo R, Villarroya J, Gavaldà-Navarro A, Giralt M. Toward an understanding of how immune cells control brown and beige adipobiology [review]. Cell Metab 2018;27:954–61.
26. Shabalina IG, Petrovic N, de Jong JM, Kalinovich AV, Cannon B, Nedergaard J. UCP1 in brite/beige adipose tissue mitochondria is functionally thermogenic. Cell Rep 2013;5:1196–203.
27. López M, Lage R, Saha AK, Pérez-Tilve D, Vázquez MJ, Varela L, et al. Hypothalamic fatty acid metabolism mediates the orexigenic action of ghrelin. Cell Metab 2008;7:389–99.
28. Metsios GS, Stavropoulos-Kalinoglou A, Douglas KM, Koutedakis Y, Nevill AM, Panoulas VF, et al. Blockade of tumour necrosis factor-α in rheumatoid arthritis: effects on components of rheumatoid cachexia. Rheumatology (Oxford) 2007;46:1824–7.
29. Binymin K, Herrick A, Carlson G, Hopkins S. The effect of disease activity on body composition and resting energy expenditure in patients with rheumatoid arthritis. J Inflamm Res 2011;4: 61–6.
30. Brooks SL, Neville AM, Rothwell NJ, Stock MJ, Wilson S. Sympathetic activation of brown-adipose-tissue thermogenesis in cachexia. Biosci Rep 1981;1:509–17.
31. Shellock FG, Riedinger MS, Fishbein MC. Brown adipose tissue in cancer patients: possible cause of cancer-induced cachexia. J Cancer Res Clin Oncol 1986;111:82–5.
32. Bing C, Brown M, King P, Collins P, Tisdale MJ, Williams G. Increased gene expression of brown fat uncoupling protein (UCP)1 and skeletal muscle UCP2 and UCP3 in MAC16-induced cancer cachexia. Cancer Res 2000;60:2405–10.
33. Tsoli M, Moore M, Burg D, Painter A, Taylor R, Lockie SH, et al. Activation of thermogenesis in brown adipose tissue and dysregulated lipid metabolism associated with cancer cachexia in mice. Cancer Res 2012;72:4372–82.
34. Muscaritoli M, Anker SD, Argiles J, Aversa Z, Bauer JM, Biolo G, et al. Consensus definition of sarcopenia, cachexia and pre-cachexia: joint document elaborated by Special Interest Groups (SIG) "cachexia-anorexia in chronic wasting diseases" and "nutrition in geriatrics." Clin Nutr 2010;29:154–9.
35. Petruzzelli M, Schweiger M, Schreiber R, Campos-Olivas R, Tsoli M, Allen J, et al. A switch from white to brown fat increases energy expenditure in cancer-associated cachexia. Cell Metab 2014;20:433–47.
36. McCarthy N. Cachexia: running on empty [review]. Nat Rev Cancer 2014;14:576.
37. Argilés JM, Stemmler B, López-Soriano FJ, Busquets S. Inter-tissue communication in cancer cachexia [review]. Nat Rev Endocrinol 2018;15:9–20.
38. Masuko K. Rheumatoid cachexia revisited: a metabolic co-morbidity in rheumatoid arthritis [review]. Front Nutr 2014;1:20.
39. Santo RC, Fernandes KZ, Lora PS, Filippin LI, Xavier RM. Prevalence of rheumatoid cachexia in rheumatoid arthritis: a systematic review and meta-analysis. J Cachexia Sarcopenia Muscle 2018;9:816–25.
40. Claret M, Smith MA, Batterham RL, Selman C, Choudhury AI, Fryer LG, et al. AMPK is essential for energy homeostasis regulation and glucose sensing by POMC and AgRP neurons. J Clin Invest 2007;117:2325–36.
41. Janig W, Green PG. Acute inflammation in the joint: its control by the sympathetic nervous system and by neuroendocrine systems [review]. Auton Neurosci 2014;182:42–54.
42. Wiberg M, Widenfalk B. Involvement of connections between the brainstem and the sympathetic ganglia in the pathogenesis of rheumatoid arthritis: an anatomical study in rats. Scand J Plast Reconstr Surg Hand Surg 1993;27:269–76.
43. Tanaka H, Ueta Y, Yamashita U, Kannan H, Yamashita H. Biphasic changes in behavioral, endocrine, and sympathetic systems in adjuvant arthritis in Lewis rats. Brain Res Bull 1996;39:33–7.
44. Lorton D, Lubahn C, Lindquist CA, Schaller J, Washington C, Bellinger DL. Changes in the density and distribution of sympathetic nerves in spleens from Lewis rats with adjuvant-induced arthritis suggest that an injury and sprouting response occurs. J Comp Neurol 2005;489:260–73.

45. Lorton D, Lubahn C, Sweeney S, Major A, Lindquist CA, Schaller J, et al. Differences in the injury/sprouting response of splenic noradrenergic nerves in Lewis rats with adjuvant-induced arthritis compared with rats treated with 6-hydroxydopamine. Brain Behav Immun 2009;23:276–85.
46. Cano G, Passerin AM, Schiltz JC, Card JP, Morrison SF, Sved AF. Anatomical substrates for the central control of sympathetic outflow to interscapular adipose tissue during cold exposure. J Comp Neurol 2003;460:303–26.
47. Morrison SF, Madden CJ, Tupone D. Central neural regulation of brown adipose tissue thermogenesis and energy expenditure [review]. Cell Metab 2014;19:741–56.
48. Lin TT, Sung YL, Syu JY, Lin KY, Hsu HJ, Liao MT, et al. Anti-inflammatory and antiarrhythmic effects of beta-blocker in a rat model of rheumatoid arthritis. J Am Heart Assoc 2020;9: e016084.
49. Kang KY, Kim YK, Yi H, Kim J, Jung HR, Kim IJ, et al. Metformin downregulates Th17 cells differentiation and attenuates murine autoimmune arthritis. Int Immunopharmacol 2013;16:85–92.
50. Son HJ, Lee J, Lee SY, Kim EK, Park MJ, Kim KW, et al. Metformin attenuates experimental autoimmune arthritis through reciprocal regulation of Th17/Treg balance and osteoclastogenesis. Mediators Inflamm 2014;2014:973986.

DOI 10.1002/art.41932

Clinical Images: The appearance of scurvy on magnetic resonance imaging

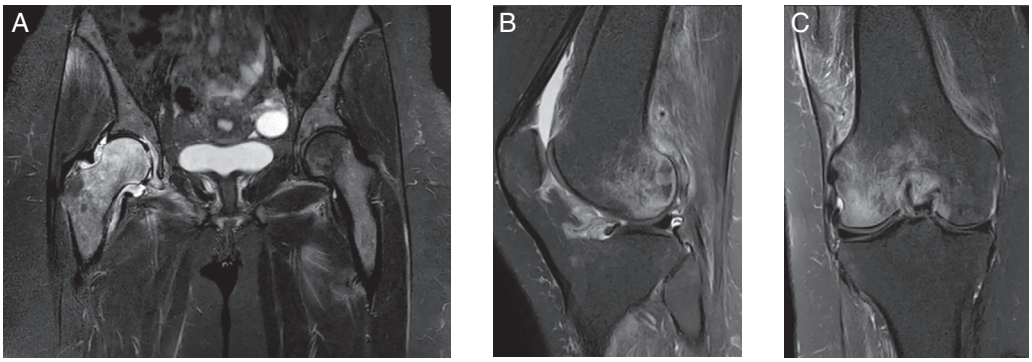

The patient, a 40-year-old woman who had been previously healthy, presented to our rheumatology department with a suspected diagnosis of arthritis based on the presence of bilateral lower limb pain, swollen knee joints, and a 6-month history of difficulty with walking. Physical examination revealed multiple subcutaneous hematomas, gingival hyperplasia, bilateral knee effusion, muscle weakness of the lower extremities, and limited movement of the right hip joint. Laboratory results were remarkable only for iron and folate deficiency with normocytic anemia (hemoglobin 9 mg/dl). A coronal STIR sequence of the hips on magnetic resonance imaging (MRI) revealed bone marrow edema in the right proximal femur (femoral head, femoral neck, intertrochanteric, and subtrochanteric regions), effusion of the right hip joint, edema of the right gluteus and bilateral proximal thigh muscles, and bilateral perifascial edema around the external obturator muscles (**A**). Similar changes were demonstrated on coronal and sagittal T2-weighted fat-saturated MRI of the right knee (**B** and **C**). Vitamin C was not detected in the patient's blood, and a diagnosis of scurvy was made. After treatment with vitamin C and multivitamins, the symptoms of scurvy resolved. Subsequently, it was found that the patient had a selective eating disorder and had restricted her diet to rice and unfortified yogurt. These MRI findings are not specific to scurvy. The appearance of the bone marrow on MRI may represent focal areas of hemorrhage or small infarcts (1). The appearance of the muscle likely represents perivascular edema and hemorrhage into the muscles and soft tissues, and effusion of the hip and knee joints may represent hemarthrosis. These clinical features and MRI findings can also be present in the setting of other, more common conditions, such as osteomyelitis, hematologic diseases, arthritis, inflammatory muscle disease, and other rheumatic and autoimmune diseases (1–3); therefore, such a symptom profile as was seen in our patient should be approached with a high index of clinical suspicion in the diagnosis and management of the disease.

Author disclosures are available at https://onlinelibrary.wiley.com/action/downloadSupplement?doi=10.1002%2Fart.41932&file=art41932-sup-0001-Disclosureform.pdf.

1. Karthiga S, Dubey S, Garber S, Watts R. Scurvy: MRI appearances. Rheumatology (Oxford) 2008;47:1109
2. Choi SW, Park SW, Kwon YS, OH IS, Lim MK, Kim WH, et al. MR imaging in a child with scurvy: a case report. Korean J Radiol 2007;8:443–7.
3. Ferrari C, Possemato N, Pipitone N, Manger B, Salvarani C. Rheumatic manifestations of scurvy [review]. Curr Rheumatol Rep 2015;17:26.

Sami Giryes, MD
Daniela Militianu, MD
Yolanda Braun-Moscovici, MD
Rambam Health Care Campus
and Technion-Israel Institute of Technology
Haifa, Israel